Review Article

Changing landscape of optical imaging in skeletal metastases

Check for updates

Nicholas Cho[a,b], Monica Shokeen[a,b,c,*]

[a] Department of Radiology, Washington University School of Medicine, 4515 McKinley Ave, St. Louis, MO 63110, United States
[b] Department of Biomedical Engineering, Washington University in St. Louis, St. Louis, MO 63110, United States
[c] Alvin J. Siteman Cancer Center at Washington University School of Medicine and Barnes Jewish Hospital, St. Louis, MO 63110, United States

ABSTRACT

Optical imaging is an emerging strategy for *in vitro* and *in vivo* visualization of the molecular mechanisms of cancer over time. An increasing number of optical imaging contrast agents and techniques have been developed in recent years specifically for bone research and skeletal metastases. Visualizing molecular processes in relation to bone remodeling in metastasized cancers provides valuable information for understanding disease mechanisms and monitoring expression of primary molecular targets and therapeutic efficacy. This review is intended to provide an overview of tumor-specific and non-specific contrast agents in the first near-infrared window (NIR-I) window from 650 nm to 950 nm that can be used to study functional and structural aspects of skeletal remodeling of cancer in preclinical animal models. Near-infrared (NIR) optical imaging techniques, specifically NIR spectroscopy and photoacoustic imaging, and their use in skeletal metastases will also be discussed. Perspectives on the promises and challenges facing this exciting field are then given.

1. Introduction

Bone is one of the most common metastatic sites of malignant neoplasms. There are over 600,000 cases of bone metastases diagnosed every year in the USA in older adults (> 40 years of age) [1]. Metastasis is characterized by severe pain, pathologic fracture, spinal compression, hypercalcemia, and ultimate mortality associated with end-stage cancers in breast, prostate, melanoma and multiple myeloma (MM) [2]. Advances in clinical imaging modalities have allowed for early detection of skeletal metastasis for accurate staging as well as implementation of optimal treatment strategies. While traditional modalities, such as planar X-ray and Computed Tomography (CT), provide structural information on calcified tissue, these modalities do not provide the functional information that is of great importance in staging metastatic tumor growth. Single Photon Emission Computed Tomography (SPECT) and Positron Emission Tomography (PET) are currently the gold standards in performing such noninvasive functional clinical imaging. SPECT, particularly bone scintigraphy, as well as PET can be used to measure tracer uptake into tissues and therapeutic effects on disease processes. While SPECT and PET are highly sensitive, there are several limitations. In addition to the use of ionizing radiation and relatively poor spatial resolution (through several millimeters) compared to magnetic resonance imaging (MRI), X-ray and CT, it is only possible to trace one molecular species with PET and does not allow for monitoring of interactions between molecular targets [3].

In preclinical skeletal cancer research, optical imaging in the first near-infrared (NIR-I) window (650–950 nm) [4] is a rapidly emerging field, with widespread applications for functional and structural imaging of the bone as well as tumors within the bone microenvironment. These techniques not only allow for multiplexing of signals, but also for evaluating interactions between specific molecular targets in relation to bone growth, the microenvironment and tumor metastasis. With advances in microscopy, small animal imaging instrumentation and novel tumor- and bone- specific contrast agents, optical imaging is a low-cost, high-throughput method of bone imaging. While we recognize the need for bioluminescence imaging (BLI) and fluorescent reporter constructs in the study of bone metastases, this review is focused on optical imaging modalities in the NIR-I window. Here, we give an overview of NIR optical imaging molecular probes, both commercial as well as in development, that are used for functional imaging of biological processes in relation to metastasized cancers to the bone. This is followed by optical imaging techniques in the NIR-I window used to endogenously image structural components of the bone and molecular processes in the bone microenvironment during metastases. We conclude with a summary and an outlook of future directions in skeletal imaging and how these various imaging techniques can be applied to characterizing bone metastases.

* Corresponding author at: Department of Radiology, Washington University School of Medicine, 4515 McKinley Ave, St. Louis, MO 63110, United States
E-mail address: mshokeen@wustl.edu (M. Shokeen).

2. Background

Tumor cells, bone cells, secreted factors, extracellular matrix, and tumor–bone interactions all play crucial roles in the growth and colonization of tumor cells in the bone microenvironment. This includes activation of angiogenic signaling pathways between tumors and stroma cells, local increases in bone turnover and osteolytic lesions, and suppression of the adaptive immune system. All of these processes provide a positive feedback cycle on tumor metastases [5]. Recent developments in NIR fluorescent contrast agents have allowed for functional imaging of these bone-related processes. NIR fluorescence also offers reduced autofluorescence *in vivo* compared to the visible fluorescence range (400 to 650 nm) in preclinical animal models [4]. Such noninvasive imaging allows for longitudinal evaluation of cancer-specific therapies without the need to sacrifice mice. Multiplexing of fluorescence signals at different emission wavelengths provides valuable functional information on how different molecular processes interact with one another and where tumor cells migrate to in real-time. Bone- and vasculature-specific NIR fluorescent agents can be co-administered to identify where tumors are growing and where biological processes involved in metastases are occurring with respect to different anatomical features *in vivo*. *Ex vivo* imaging of excised tissue allows researchers to locate where a receptor or protein of interest is expressed on the tumor cell and simultaneously evaluate different molecular processes in the context of individual cells.

Despite the advantages offered with NIR fluorescent contrast agents, the fundamental limitations associated with fluorescent imaging need to be considered when performing such imaging. High photon scattering and tissue attenuation limit translation of these agents into humans for noninvasive imaging, particularly for skeletal imaging. While fluorescent contrast agents provide valuable functional information, these agents do not provide the same structural or compositional information that is offered by other anatomical imaging modalities. Questions regarding tumor depth and shape, for example, are highly dependent on the tissue scattering properties and depth of tissue [6,7], and therefore cannot be accurately determined solely using NIR fluorescence as compared to X-ray, CT or MR imaging. Spectral overlap between different fluorophores also limits the number of processes that can be evaluated at any one time. Fluorophores must be chosen such that emission peaks are preferably 20 nm apart from one another, limiting the potential number of contrast agents that can be administered at any one time [8]. However, successful examples exist, such as the work by Kobayashi et al. who demonstrated simultaneous multicolor imaging of 5 different NIR contrast agents *in vivo* [8]. With recent advances in targeting moieties and improved technologies for real-time fluorescence imaging in small animal models, NIR fluorescent agents have pushed the field forward and can provide valuable functional information on biological processes involved in bone metastases and associated therapies in preclinical animal models. Here, we evaluate several tumor- and bone-specific NIR tracers as defined by their primary target (shown in Table 1 and Fig. 1).

2.1. Functional imaging of biological processes involved in bone metastases

2.1.1. Metabolism

One of the hallmarks of tumor cell development is an elevated rate of glycolysis, even under aerobic conditions [9]. This increased demand for glucose and subsequent increased production of cellular metabolites leads to the recruitment of macrophages and other immune cells that promote metastasis [10]. Aerobic glycolysis is often stimulated by oncogenes, such as *PIK3* and *Ras,* which induce the upregulation of glucose transporter proteins (GLUT), in particular *GLUT1*, and allows for trafficking of glucose into the tumor cell [11]. IRDye800CW 2-DG (Li-Cor) exploits this family of transporter proteins using the stable glucose analog 2-deoxyglucose (2-DG) [12]. IRDye800CW is a NIR dye (Ex./Em. 774 nm/810 nm) that exhibits deeper tissue penetration and a higher photostability than Cyanine 5.5 (Cy5.5) (Ex./Em. 684 nm/710 nm) due to the longer excitation wavelength [13]. IRDye800CW can be functionalized with either an N-hydroxy succinimide (NHS) ester or maleimide reactive group, allowing it to be attached to a number of biomolecules for targeting to an amide group [13].

Fluorescence microscopy confirmed dose-dependent uptake of IRDye800CW 2-DG in the cytoplasm of various tumor cell lines [12]. *In vivo* studies have shown high specificity of IRDye800CW 2-DG in tumor-bearing regions, which were verified with BLI and MRI [14]. *In vivo* BLI signals were found to be linearly correlated with fluorescence imaging from IRDye800CW 2-DG [15]. In addition, areas of low oxygen concentration or hypoxic regions also play a role in the heterogeneous uptake of the probe with higher uptake of IRDye800CW 2-DG observed in hypoxic tumor regions [16]. While the molecular mechanism by which IRDye800CW 2-DG enters the tumor cell is not entirely known, it is believed that the GLUT/IRDye800CW 2-DG complex is endocytosed into the cell following binding [12]. IRDye800CW 2-DG has not been specifically studied in bony metastatic models. Despite possible uptake of IRDye800CW 2-DG in non-specific areas of high glucose avidity, it serves as a good potential candidate for characterizing metabolic activity in tumor cells residing in bone both *in vivo* and *ex vivo*.

2.1.2. Adhesion

Integrin-mediated contacts with the extracellular matrix and stromal cells play a defining role in the pathogenesis of bone metastases. Overexpression of integrin signaling by cancer cells further promotes proliferation within the bone microenvironment [17]. The activated form of the receptor VLA-4 (Very Late Antigen-4, also known as $\alpha_4\beta_1$) plays a vital role in mediating adhesion of hematopoietic cells, primarily MM tumoral cells, to the bone marrow (BM) stroma and promoting tumor cell trafficking, proliferation and drug resistance [18]. Adhesion of VLA-4 to its targeting ligand VCAM-1, which is overexpressed on the surface of endothelial cells, promotes bone metastases, suggesting this interaction mediates homing of tumors to the bone [19]. LLP2A is a high-affinity peptidomimetic ligand for the activated conformation of VLA-4. Fluorescently-conjugated LLP2A has shown promise as an imaging agent in MM, lymphoma and leukemia models

Table 1
Various optical imaging probes and their associated primary targets.

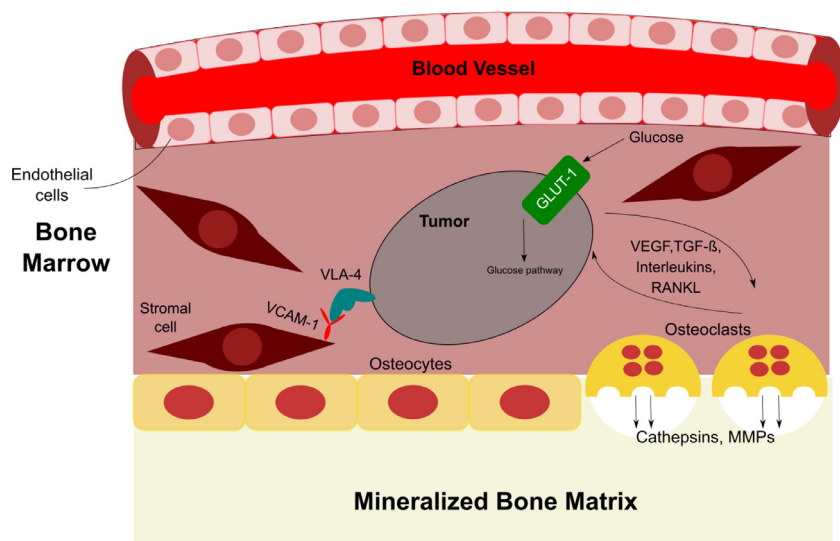| Cell type	Mechanism of action	Ligand	Tracer	Used in models of bony metastasis or intramedullary tumors?	Publication
Tumors	Cell metabolism	GLUT Transporter	IRDye800CW 2-DG	No	–
	Adhesion factors	VLA-4	LLP2A-Cy5/Cy5.5/AF680	Yes	[20]
	Angiogenesis	Blood Pool	AngioSense	Yes	[30,31]
Osteoclasts		Hydroxyapatite	OsteoSense	Yes	[33,36–40]
			BoneTag	No	–
			Cy5.5-iminodiacetates	No	–
	Bone degradation	MMP	MMPSense	No	–
		Cathepsin B	GB123	Yes	[40]
		Cathepsin K	CAT K FAST 680/750	Yes	[36]
			ProSense	No	–

Fig. 1. Tumor to bone interactions during skeletal metastasis. Schematic of the associated factors and receptors that promote bone fractures and metastasis.
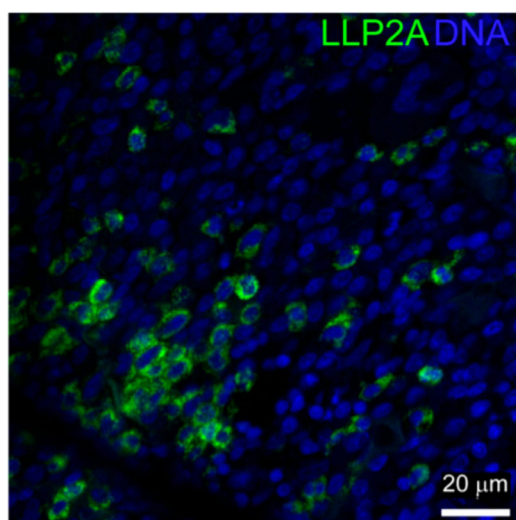

Fig. 2. Representative image of MM patient BM sample stained with LLP2A-Cy5. LLP2A exhibited punctate staining around the cell periphery, consistent with it labeling VLA-4. LLP2A staining is shown in green and 4′6-diamidino-2-phenylindole (DAPI) labeling of nuclei in blue (This research was originally published in JNM. Soodgupta, D., et al. Ex vivo and In Vivo Evaluation of Overexpressed VLA-4 in Multiple Myeloma Using LLP2A Imaging Agents. J Nucl Med. 2016; 57: 640–645. © SNMMI).

[20–22]. *In vitro* imaging of LLP2A showed specific surface binding on $\alpha_4\beta_1$ expressing tumor cells in human BM samples (Fig. 2) [20]. *In vivo* imaging of LLP2A was studied in mouse xenograft models and showed high sensitivity and specificity with fast clearance through the kidneys [20–22]. This is a promising approach for visualizing changes in cell adhesion-mediated tumor interactions within the bone microenvironment in preclinical models.

2.1.3. Angiogenesis

The interaction of metastasized tumor cells with extracellular matrix (ECM) proteins and BM cells, as well as in the BM milieu, play a crucial role in tumor pathogenesis and drug resistance [23–25]. Tumors, particularly MM tumoral cells, are characterized by widespread involvement of the BM at diagnosis, implying circulation into the peripheral blood and trafficking of tumor cells into new sites of the BM *via* chemokines and other signaling cascades [26,27]. Methods to track bone metastasized tumor cells, both in the BM and circulation, are

valuable for developing new therapeutic strategies to target malignant cells in the bone microenvironment.

While angiogenesis is a critical marker of tumorigenesis, delineating tumor masses from healthy BM solely with angiogenic markers can be extremely challenging due to the highly vascularized nature of the BM microenvironment [28,29]. Angiogenic-specific NIR contrast agents, however, can be used as an anatomical marker for blood vessels in conjunction with other tumor-specific contrast agents or tumor cells expressing a fluorescent protein. AngioSense (Perkin Elmer) has been used in imaging BM vasculature in relation to intramedullary tumors in MM. The agent is a fluorescently-labelled, long-circulating synthetic graft polymer conjugated to either the fluorophore VivosTag680 (AngioSense680; Ex./Em. 680 nm/700 nm) or VivosTag750 (AngioSense750; Ex./Em. 750 nm/770 nm). Runnels et al. used AngioSense750 in order visualize early MM cell division along vasculature in regions adjacent to marrow spaces. By transfecting green fluorescent protein (GFP) constructs into human myeloma cells, noninvasive *in vivo* flow cytometry and confocal microscopy were used to follow engraftment of MM cells in the BM vasculature in immunocompromised mice. MM cells were found closely associated with normal marrow vasculature adjacent to marrow spaces infiltrated with tumor, suggesting that vasculature plays a significant role in the dissemination of the disease in the BM [30]. Using similar imaging techniques, Azab et al. also used AngioSense750 to image the blood vessels in the BM niches of MM murine models. AMD3100 is a small molecule inhibitor that prevents homing of MM cells to the BM. By multiplexing with markers for cell viability and apoptosis in conjunction with fluorescently-labelled blood vessels, the authors could visualize apoptotic MM cells in the circulation of mice treated with AMD3100 and a frontline MM therapy, bortezomib [31].

2.2. Optical imaging of the skeleton and skeletal processes

2.2.1. Osteoclasts

There are two major, commercially-available NIR fluorescent imaging probes specific to the skeleton. Such bone-specific fluorophores may be administered in conjunction with other tumor-specific fluorophores in order to visualize the bone anatomy *via* multiplexing of signals. By using different fluorophores of different emission wavelengths, areas of metastasis in murine models can be identified in relation to bone regions [32].

OsteoSense (Perkin Elmer) is one of the most commonly used preclinical contrast agents for imaging the bone *in vivo*. OsteoSense is a
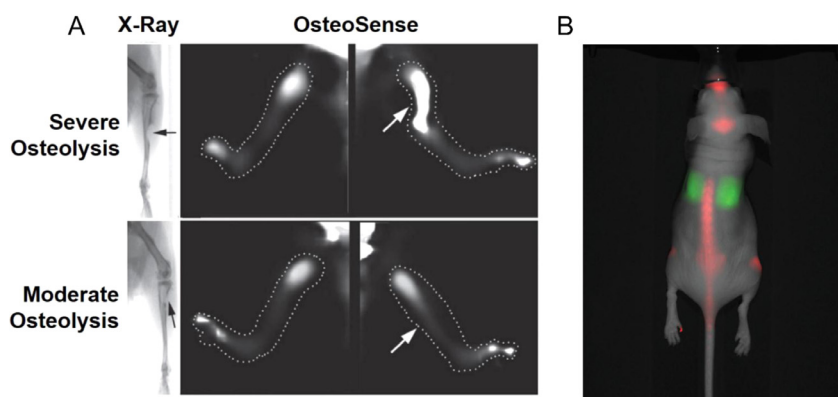
Fig. 3. Representative images of osteoclast-specific fluorescent probes in metastatic murine models. A) Mice receiving intratibial injections of PC-3 prostate cancer cells, leading to variable degrees of osteolysis 24 days post-injection. X-ray (left) was performed to confirm fractures (shown in black arrows). *In vivo* FMT imaging of OsteoSense (right) revealed fluorescent binding in mice progressing to fracture, but not in mice with only moderate osteolysis. Dotted lines represent tibial and foot outlines guided by planar fluorescent and white-light images taken before FMT scan. White arrows indicate corresponding fracture location *in vivo* (Adapted from [33]) B) MDA-MB-231 breast cancer injected intracranially 3 weeks prior to administration of IRDye BoneTag (shown in red) and IRDye800CW EGF (shown in green). BoneTag has been used to visualize the bone anatomy/structure in conjunction with secondary optical agents specific for a primary target (Copyright, LI-COR, Inc., used by permission).

fluorescently-labelled bisphosphonate, a class of drugs targeting the hydroxyapatite (HA)-active regions on the mineralized bone surface, where they are taken up by osteoclasts [33,34]. This probe is available with different excitation and emission wavelengths: OsteoSense680 (Ex./Em. 680 nm/700 nm), OsteoSense750 (Ex./Em. 750 nm/780 nm) and OsteoSense800 (Ex./Em. 780 nm/805 nm). OsteoSense has shown strong and long-lasting specificity *in vivo* and has been correlated with differential expression of HA, bone size and rate of bone remodeling [35]. OsteoSense has shown to accumulate in areas of high bone turnover, indicating bone lesion activity and has been used in monitoring osteoclast activity in bone metastatic cancer models [33]. Primary prostate and breast cancers metastasized to the bone have been explored using this imaging probe. Kozloff et al. intratibially implanted PC-3 cancer cells into mice to assess OsteoSense binding in a bone resorption model [33]. Fluorescence Molecular Tomographic (FMT) imaging showed increased binding in mice with severe osteolysis, but not in mice with moderate osteolysis. Fractures were confirmed *via* X-ray imaging (Fig. 3A).

OsteoSense has also been used in longitudinal therapy studies in skeletal metastatic animal models for noninvasive imaging of bone reformation *in vivo*. Gálban et al. intratibially injected MDA-MB-231 human breast cancer cells into immunocompromised mice. Following weekly administration of the therapy docetaxel, mice were subsequently administered OsteoSense800 as the primary diagnostic probe to functionally assess bone remodeling in treated and untreated groups [36]. Progressive increases in relative OsteoSense800 signal for treated groups compared to control groups indicated upregulated osteoblastic activity and improved bone reformation.

Although OsteoSense has been the sole fluorescent probe administered in bone metastatic models, it can also be co-administered in conjunction with other tumor-specific markers to visualize bone anatomy and spatially identify where tumors are metastasizing with respect to the bone [37–40]. Imamura et al. transplanted fluorescently-transfected human breast cancer cells in bone metastatic murine models to visualize the cell cycle of cancer cells *in vivo* [38]. Intravital microscopy was used to noninvasively image metastasized tumor cells in the S/G/M2 phase in female nude mice. OsteoSense750 was co-administered to stain for bone to visualize where tumor cells were growing *in vivo*. Fluorescent visualization of the bone allowed researchers to co-register fluorescence emitted at different wavelengths and to validate where tumor-specific fluorescence is emitting from *in vivo*.

While bisphosphonates have high affinity for bone surfaces, these compounds have shown to induce osteoclast-induced apoptosis, leading to high bone turnover [41,42] and osteonecrosis [43]. This limits long-term storage of bone tissue stained with OsteoSense. To overcome this limitation, recent advances have been made towards peptide-based imaging agents that are both derived from and specific to natural bone-binding proteins. BoneTag (Li Cor BioSciences) is a tetracycline derivative, conjugated to IRDye800CW as well as IRDye680 (Ex./Em.

680 nm/700 nm), that targets mineralized bone matrix as a calcium chelator [44]. BoneTag has also been used to study osteoblastic activity in osteoarthritis [45] as well as coronary atherosclerotic murine models [46] due to the active expression of HA in these disease models. While OsteoSense as well as BoneTag have shown positive correlation with Alizarin Red S staining and reduced autofluorescence *in vivo*, BoneTag is more specific under conditions of low mineralization [47]. In addition, BoneTag can be stored for up to a year without losing specificity compared to the limited storage time of 8 weeks with OsteoSense [47]. While BoneTag has yet to be tested in the presence of bone metastatic cancers, there is great potential for skeletal imaging and measuring osteoblastic activity in these models, particularly in the presence of genetic modifications as well as cancer therapies specific to bone metastasis. Similarly to OsteoSense, BoneTag may also be administered in conjunction with other tumor-specific fluorophores in order to identify regions of tumor metastasis within mice (Fig. 3B).

Another class of peptides, iminodiacetates, imitate the bidentate structure of one of the side chains of osteocalcin. Osteocalcin is a protein that binds to HA amino acid residues and is produced by osteoblasts during bone formation and healing. Harmatys et al. [48] and Pes et al. [49] have demonstrated the feasibility of fluorescently-conjugated iminodiacetates for skeletal imaging in metastasized breast cancer models. *In vivo* studies have shown higher uptake at 19 days with a tetra-iminodiacetate moiety, conjugated to Cy5.5 dye, than the uptake from OsteoSense750 while exhibiting high renal clearance from this moiety within hours of injection [48]. While these imaging agents have yet to be evaluated in bony metastatic models, future work with small molecule agents or nanoprobes using a multivalent iminodiacetate group has promise as bone targeting agents.

2.2.2. Matrix degradation

Various factors participate in the vicious cycle in which cancer cells are stimulated to promote pro-osteolytic factors, causing bone loss and fracture. Fluorescent approaches have emerged to image matrix degradation and local inflammation and typically involve selective cleavage of fluorescently-conjugated macromolecules by cathepsins or matrix metalloproteinases (MMPs) for fluorescence to be released. These contrast agents primarily rely on self-quenching upon binding to the target of interest. Several fluorophores are in close proximity to each other on the targeting macromolecule and the small distance between the fluorophores leads to quenching of the fluorescent signal. When the ligand is enzymatically digested, the fluorophores are released. The fluorophores are no longer quenched and the signal can be detected with fluorescence imaging equipment.

Cathepsins are a family of proteases expressed by active osteoclasts and are involved in the breakdown of the bone matrix. Cathepsins B (Cat B) and K (Cat K) recruit macrophages that further promote tumor metastases and are highly present within osteolytic lesions and sites of osteoclastic bone resorption [50]. ProSense (Perkin Elmer) is an
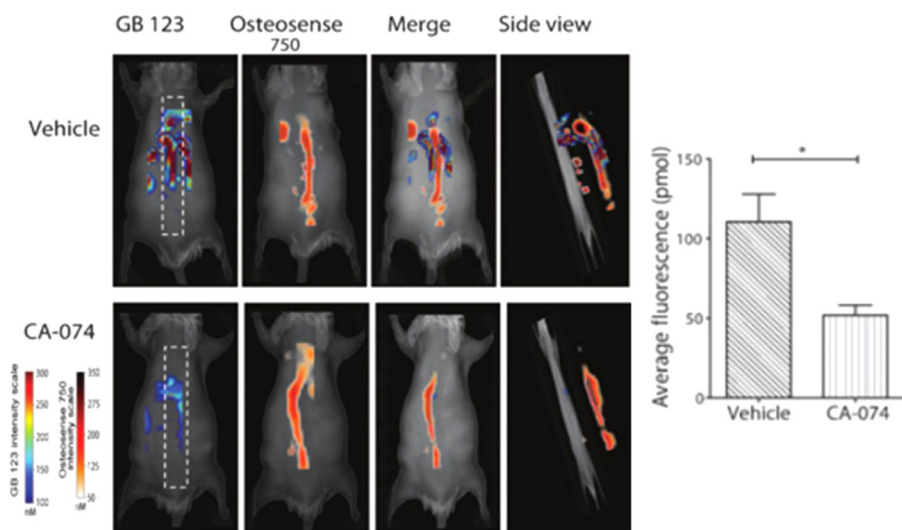
Fig. 4. *In vivo* imaging of Cat B activity in tumor-burdened mice. Fluorescence spinal images of live mice-bearing 4T1.2 breast tumors treated with vehicle or with Cat K inhibitor CA-074 followed by administration of the Cat B-specific fluorophore GB123 and Osteosense750. Quantitation of mean GB123 fluorescence signal in vehicle and CA-074-treated spines with the FMT2500 system showed decreases in Cat B activity following inhibition (Adapted from [40]).

enzyme-activated fluorescent agent hydrolyzed by several cathepsins, preferentially Cat B. ProSense has demonstrated utility in imaging Cat B$^+$ macrophage infiltration within preclinical colon cancer animal models [51,52]. Withana et al. noninvasively evaluated the efficacy of Cat B inhibition *via* the small molecule inhibitor CA-074 in order to treat metastatic breast cancer [40]. GB123 is a Cat B-specific activity-based fluorescent contrast agent (Ex./Em. 633 nm/680 nm) and was used to evaluate expression of Cat B *in vivo*. Using the fluorescent diphosphonate probe OsteoSense750, cysteine cathepsin activity was co-registered along the spine of mice bearing breast tumors metastasized to the bone (Fig. 4). This activity was reduced in mice treated with CA-074 and showed decreased metastasis in lung and bone regions.

Similar contrast agents are available that contain a slightly different backbone or linker sequence resulting in specificity for other proteases. Using a cleavable Cat K probe that consists of an amino acid backbone chain functionalized with Cy5.5 fluorophores through the Cat K-sensitive link sequence, Kozloff et al. first demonstrated noninvasive visualization of bone-degrading enzymes in models of accelerated bone loss [53]. Cat K Fluorescent Activatable Sensor Technology (FAST) is another cleavable probe specific to Cat K. Cat K 680 FAST (PerkinElmer) was developed based on a human Cat K-cleavable sequence, a pair of self-quenching NIR fluorochromes and a pharmacokinetic modifier to confer increased blood half-life. The agent is optically quenched in its native form, but upon cleavage by Cat K, it becomes highly fluorescent (Ex./Em. 674 nm/692 nm). Cat K FAST has shown promising results in specific imaging of the biological activity of regions of bone resorption and osteocytes in osteoarthritic models [54].

Matrix Metalloproteinases (MMPs) are important factors associated with remodeling of the tumor microenvironment and local activation of the immune system. MMPs have been implicated in mediating expression of Receptor Activator of Nuclear factor Kappa-B Ligand (RANKL), promoting osteolysis and metastases to the bone [55]. MMPs are also involved in regulating angiogenesis through release of Vascular Endothelial Growth Factor (VEGF) and Epidermal Growth Factor (EGF)-like factors [56]. MMPSense (Perkin Elmer) is a small molecular polypeptide (GPLGVRGKC) conjugated to a pegylated polylysine scaffold and is fluorescent upon enzymatic cleavage, predominantly from MMP 7, 9 12, and 13. This MMP probe has been used to visualize local proteinase activity and macrophage activation in diseases like atherosclerosis [50] as well as osteoarthritis [57,58]. In summary, imaging proteinase-activated fluorescent probes can provide functional information on interactions between the tumor microenvironment, osteoclastic bone resorption and local inflammation.

2.3. NIR skeletal imaging techniques

In the following sections, we provide an overview on recent advances of Raman and NIR spectroscopy as well as photoacoustic tomography (PAT) in the imaging of bone metastases. These modalities rely on noninvasive, label-free imaging of endogenous tissue contrast *via* NIR laser excitation, allowing for real-time imaging of molecular processes. Each of these techniques offers unique information on bone tissue not offered by NIR fluorescent probes. Raman spectroscopy provides chemical information on the structure of bone such as mineral phosphate, carbonate, matrix collagen, and bone water content. These measurements can serve as metrics for bone fragility and density in the context of bone metastasis and reveal how bone strength and mechanics are affected when fracturing occurs following tumor-induced osteolysis.

PAT, conversely, can offer physiological information on a tumor and its location with respect to the bone using endogenous contrast. Because PAT imaging relies on light propagation in one direction, the depth and shape of a tumor can be more accurately determined than solely with NIR contrast agents. In addition, environmental changes surrounding the tumor in the BM microenvironment can be evaluated in real-time. Metabolic rate of oxygen consumption and lipid content are some of the parameters that can be measured *in vivo* using endogenous contrast. If tissue absorptivity is known, concentrations of these endogenous chromophores can also be quantitatively assessed and can serve as metrics for molecular processes in the context of metastases. Due to weaker ultrasound scattering and unique optical absorption contrast from hemoglobin and other tissue, PAT can provide valuable molecular information at clinically relevant depths and at high resolution. Exogenous contrast agents in the NIR-I window specific to the BM can further enhance this resolution.

There are still several technical limitations with NIR spectroscopy and PAT. Because these imaging techniques rely primarily on endogenous contrast, there are a number of considerations to make to attain optimal signal. In the case of Raman spectroscopy, heterogeneity of optical fluence and competing tissue autofluorescence may also compete with Raman scattering and can hamper the interpretation of Raman spectra in biological samples. As for PAT, spectral overlap as well as sensitivity of different endogenous chromophores may interfere with image acquisition. While current efforts for both forms of optical imaging in skeletal metastases are either limited to *ex vivo* bone imaging or to imaging of primary tumors not metastasized to the bone, advancements in hardware design, reconstruction algorithms and novel contrast agents are allowing these techniques to compete with traditional imaging modalities. Technical improvements in system implementation and reconstruction algorithms will be key in order to

improve sensitivity, including faster scanning mechanisms and higher frequency lasers with a wide tuning range of wavelengths for real-time functional imaging. Comprehensive spectral databases and tissue classification methodologies that can be compared with current gold standards will be needed to validate spectroscopic datasets. Here, we highlight both NIR spectroscopy and PAT and their potential in evaluating tumors metastasized to the bone.

2.3.1. NIR spectroscopy

Raman spectroscopy is a form of vibrational spectroscopy that detects scattered light from chemical bonds and biological molecules upon excitation by NIR laser light. This light interacts with low-frequency vibrational photons, resulting in the inelastic scattered photons being shifted in energy to values different than that of the excitation. This shift is measured in terms of the difference between the inverse of the excitation and detected wavelengths (units: cm^{-1}) and gives information that is specific to chemical bonds. Raman spectroscopy depends on the polarizability of a molecule and is more sensitive to homo-nuclear bonds [59]. The resulting spectra provides a fingerprint by which different molecular species can be identified and their relative concentrations evaluated based on the strength of different peaks. Biological tissues contain a large number of Raman-active molecules, resulting in spectroscopic measurements that are in effect a weighted sum of spectra from all molecular species within a tissue.

Raman spectroscopy has been used to characterize bone composition in relation to bone strength and allows for analysis of intact samples in a hydrated state without additional processing of bone tissue [59]. Phosphate, amide I and mineral carbonate are some of the most commonly detected bonds in the bone matrix [60]. While phosphates (~ 959 cm^{-1}) are characteristic of the HA in the bone matrix, amide I (1616 –1720 cm^{-1}) and mineral carbonate (1070 cm^{-1}) are both measures of collagen structure [61]. Ratiometric measurements of the band intensities with respect to the bond peaks are calculated as either a mineral/matrix, carbonate/phosphate or collagen cross-link ratio. These ratios can be used to assess bone remodeling and compositional trends in various bone specimens and disease models [59]. In the area of cancer metastases, Raman spectroscopy has been used to evaluate bone mineral content in metastasized breast and prostate cancer models. In metastasized breast cancer, phosphate/amide I ratio as well as carbonate/phosphate ratios increased in the bone with increasing tumor burden and bone lesion size, suggesting an increase in mineral density and reduction in bone toughness in the presence of tumors (Fig. 5A) [62]. Similarly, in metastasized prostate cancer models, carbonate/phosphate ratios were greater in tumor-bearing bones while carbonate/matrix ratios significantly decreased, suggesting that the presence of tumors elevated bone turnover rate instead of a synergetic change with bone mineralization (Fig. 5B) [63,64]

In addition to bone mineral density and collagen, water content and hemodynamics within the bone have been evaluated with NIR spectroscopy (NIRS). While NIRS has a lower resolution limit compared to Raman due to its broader spectral features and lower intensities, NIRS absorption bands arise from molecular vibrations of C−H, C−O, O−H and N−H bonds, allowing for monitoring of water content, lipids, hemoglobin and proteins [65]. These are features unattainable through Raman spectroscopy. Water distribution in BM serves as endogenous contrast in MRI for detecting and characterizing lesions. NIRS was shown to have similar resolution to ultra-short echo time MRI when free bone water as well as water-bound collagen was evaluated in cadaver human tibiae *ex vivo* [66]. NIRS has also been used in the evaluation of oxygenated and deoxygenated bone tissue *in vivo* [67]. In addition to hemodynamics and water, studies have also been conducted in evaluating lipid and protein content within soft tumor tissue in a variety of cancers, primarily breast cancer. Additional information on NIRS in cancer can be found at ref [68]. In summary, Raman and NIR spectroscopy have great potential in characterizing biochemical components of bone structure and can be related to fracture risk and lesions in the presence of metastasized tumors.
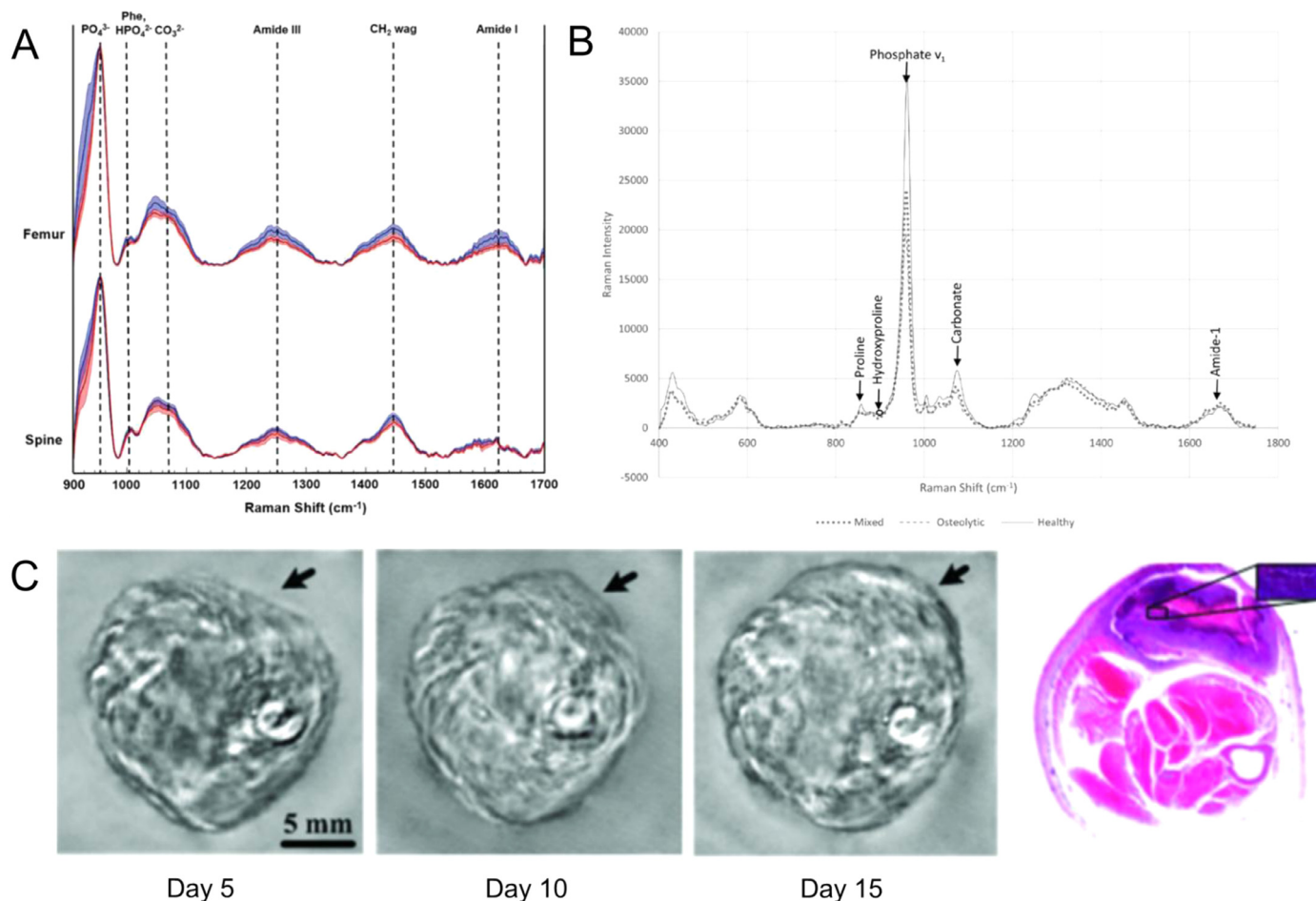
2.3.2. Photoacoustic tomography

Photoacoustic Tomography (PAT) is a hybrid imaging modality that is based on the acoustic detection of optical absorption from biological tissue exposed to a pulsed laser. Following absorption of light by the tissue, the absorbed light is converted into heat, resulting in the expansion of thermoacoustic waves. Biological tissues contain several kinds of endogenous chromophores such as hemoglobin, melanin and lipids which have strong absorptivity when excited at the appropriate wavelengths [69]. These endogenous contrast agents allow for monitoring of physiological changes such as oxygen saturation and vascular blood volume in association with these chromophores. Multispectral imaging of malignant tumors has been performed within a wide variety of preclinical and clinical studies including: breast, skin, prostate, and ovarian. Vasculature and oxygen saturation within the tumor tissue have been characterized for detection of angiogenesis [70]. Imai et al. used optical-resolution photoacoustic microscopy (PAM) to non-invasively quantify total oxygen saturation (sO$_2$) and vascularization during MM progression. *In vivo* PAM of the cerebral BM in immunocompromised mice, following MM cell injection, showed that MM tumor regions had significantly lower total sO$_2$ concentrations and blood vessel densities than in non-tumor affected regions. This demonstrated both the development of hypoxia due to MM cell proliferation and decreased vascularization surrounding the tumor areas [71]. Detection of metastatic tumors as well as circulating tumor cells (CTCs) have also been performed with PAT-based flow cytometry. Guiettez-Juarez et al. [72] and Galanzha et al. [73] both detected 1 CTC/1 mL of blood *in vivo* and Juratli et al. [74] has shown that manipulation of tumors such as pressure, biopsy and laser treatment can dramatically increase CTC counts and cancer metastasis.

In addition to endogenous contrast imaging, exogenous agents utilizing NIR dyes as well as nanoparticles have been used to enhance the contrast of tumor tissue *in vivo*. Non-specific and specific contrast agents have been designed for this purpose. NIR-absorbing dyes such as IRDye800CW [75], AlexaFluor740 [76], and indocyanine green (ICG) [77,78] have served as PAT contrast agents. Metal particle-based contrast agents, primarily gold nanoparticles, have also been used to enhance PAT contrast. Gold has become a metal of choice due to its high absorption coefficient, thermal conductivity, and surface plasma resonance [79] and has shown concentration-dependent enhancement in signal-to-noise ratio and resolution [80]. While PAT has yet to be extensively studied in bone cancer metastases, early efforts have been made in using PAT to enhance tumor contrast in preclinical osteosarcoma models (Fig. 5C) [81,82]. PAT has also been studied in *ex vivo* imaging of vasculature in bone tissue in arthritic rat models as well as human cortical bones with high contrast and resolution [83,84]. Various configurations of pulsed laser diodes have been designed to excite endogenous HA and hemoglobin in the NIR-I window [85]. With multispectral imaging, in conjunction with NIR probes specific for targets within the tumor, PAT could provide valuable insight into tumor interactions with the bone microenvironment, specifically in relation to changes in hemoglobin content.

2.4. Conclusions and future directions

Bone metastases is a complex process that can ultimately lead to mortality if left untreated. It is therefore integral to understand the complicated mechanisms underlying skeletal metastasis and to develop better methods of monitoring therapy *in vivo*. Optical imaging is a promising tool in understanding this disease's pathogenesis and its associated therapies.

In the area of NIR fluorescent compounds, there are still a host of factors that could serve as potential targets for imaging. New tracers targeting different molecular signatures, and therefore biologic properties of bone metastasis, will enhance knowledge of disease

Fig. 5. Raman spectroscopy and photoacoustic tomographic imaging allow for label-free imaging in primary and metastasized bone cancer models. A) Representative Raman spectra acquired from metastatic cancer-affected femurs and spines. Spectra (normalized to PO_4^{3-} v_1 peak) were acquired from week 0 control group (blue tracings) and 5 weeks after tumor inoculation (red tracings). The solid lines represent the mean spectrum of each sample group with associated shadings representing ± 1 standard deviations (SD). The distinctive Raman peaks at 958, 1004, 1070, 1250, and 1450 cm^{-1} suggest changes in carbonate substitution, overall mineralization as well as crystallinity increases in tumor-bearing bones [62] – Published by The Royal Society of Chemistry. B) representative Raman spectra of spines in control mice (healthy) and mice inoculated with HeLa cervical or Ace-1 prostate cancer cell lines producing osteolytic or mixed (osteolytic and osteoblastic) metastases, respectively (Adapted from [63]). C) Noninvasive *in vivo* photoacoustic imaging of osteosarcoma in a rat leg between 5 and 15 days after tumor inoculation. Arrows show tumor suspicious areas. Histological images of a cross section of the rat leg 15 days after imaging show tumor suspicious area (Adapted from [81]).

progression. Chemokines play a central role in lymphocyte trafficking and homing, specifically the chemokine receptor 4 (CXCR4). Previous studies have shown that CXCR4 plays a critical role in homing of MM tumoral cells to the BM. Inhibition of the receptor not only prevents migration of MM cells, but also sensitizes malignant tumor cells to therapeutic agents [86]. Tumor Growth Factor-β (TGF-ß) and RANKL are two prominent soluble factors involved in stimulation of pro-osteoclast formation [87]. RANKL activates osteoclast-mediated bone resorption and subsequently promotes the release of matrix growth factors such as TGF-ß, further inducing tumor growth in a positive feedback mechanism [87]. Adipocytes are another important component in the BM environment and in bone metastases. Marrow adipocytes secrete factors that have profound effects on the BM niche, inflammation, and homing of tumor cells to the microenvironment [1]. Several receptors such as FABP4 and acetate have been identified in promoting tumor growth and could serve as potential targets for noninvasive imaging in preclinical animal models.

While NIR fluorescence offers valuable functional information in preclinical animal models, there is limited translatability for noninvasive skeletal imaging in humans due to the high tissue attenuation of bone. NIR spectroscopy and PAT have emerged as potential noninvasive imaging modalities for cancer imaging. Due to the reduced tissue autofluorescence and lower tissue scattering observed in this wavelength spectrum, both imaging modalities have the potential for translation into humans. While Raman spectroscopy and PAT have not been studied in the context of bone metastatic models, these modalities have entered the clinic for imaging of primary tumors in humans. Jermyn et al. demonstrate the use of Raman spectroscopy in distinguishing cancer masses in late stage gliomablastoma patients [88]. This Raman-based probe, through excitation of different molecular species such as DNA and cholesterol, enabled detection of previously undetectable diffusely invasive brain cancer cells at cellular resolution in patients. Wang et al. demonstrated the first use of PAT, in combination with CT, to noninvasively image primary breast tumors in breast cancer patients [89]. Using endogenous hemoglobin, the authors were able to distinguish, at high spatiotemporal resolution, breast tumor by detailing tumor associated angiogenesis without the need for ionizing radiation or exogenous contrast agents. Limitations in the clinical translatability of these techniques will primarily involve pushing the depth penetration of these optical technologies further to overcome the high tissue attenuation of bone and surrounding heterogeneous tissue such as muscle and fat. With advances in higher frequency laser instrumentation, probe design and reconstruction algorithms, and in combination with ultrasound and CT, both imaging modalities have

great potential towards noninvasive imaging of bone metastases in humans.

In conclusion, optical imaging is an important tool for evaluating disease progression and response monitoring in preclinical models. Various imaging approaches in the NIR-I window have been developed to detect molecular processes involved in bone metastases and in relation to the bone and its microenvironment. Each technique has its own unique advantages and disadvantages for revealing fundamental biological mechanisms involved in these processes and how therapies can alter these mechanisms. In combination with ultrasound, CT, PET, SPECT and MRI, optical imaging is beginning to see rapid clinical translation and is enabling real-time assessment of tumor growth and stromal interactions on a functional, structural and molecular level. The benefits of these tools in the context of bone metastases make further investigation in this field worthwhile and needed.

Conflicts of interest statement

The authors declare that there are no conflicts of interest.

Acknowledgments

References

[1] J.Y. Krzeszinski, Y. Wan, New therapeutic targets for cancer bone metastasis, Trends Pharmacol. Sci. 36 (2015) 360–373, https://doi.org/10.1016/j.tips.2015.04.006.

[2] S. Tsuzuki, S.H. Park, M.R. Eber, C.M. Peters, Y. Shiozawa, Skeletal complications in cancer patients with bone metastases, Int. J. Urol. 23 (2016) 825–832, https://doi.org/10.1111/iju.13170.

[3] W.W. Moses, Fundamental limits of spatial resolution in PET, Nucl. Instrum. Methods Phys. Res. Sect. A Accel. Spectrom., Detect. Assoc. Equip. 648 (2011) S236–S240, https://doi.org/10.1016/j.nima.2010.11.092.

[4] A.M. Smith, M.C. Mancini, S. Nie, Bioimaging: second window for *in vivo* imaging, Nat. Nanotechnol. 4 (2009) 710–711, https://doi.org/10.1038/nnano.2009.326.

[5] W. Lin, M. Karin, A cytokine-mediated link between innate immunity, inflammation, and cancer, J. Clin. Invest. 117 (2007) 1175–1183, https://doi.org/10.1172/JCI31537.

[6] J.P. Miller, D. Maji, J. Lam, B.J. Tromberg, S. Achilefu, Noninvasive depth estimation using tissue optical properties and a dual-wavelength fluorescent molecular probe *in vivo*, Biomed. Opt. Express. 8 (2017) 3095, https://doi.org/10.1364/BOE.8.003095.

[7] V. Ntziachristos, Going deeper than microscopy: the optical imaging frontier in biology, Nat. Methods 7 (2010) 603–614, https://doi.org/10.1038/nmeth.1483.

[8] H. Kobayashi, M. Ogawa, R. Alford, P.L. Choyke, Y. Urano, New strategies for fluorescent probe design in medical diagnostic imaging, Chem. Rev. 110 (2010) 2620–2640, https://doi.org/10.1021/cr900263j.

[9] N.N. Pavlova, C.B. Thompson, The emerging hallmarks of cancer metabolism, Cell Metab. 23 (2016) 27–47, https://doi.org/10.1016/j.cmet.2015.12.006.

[10] G. Pascual, D. Domínguez, S.A. Benitah, The contributions of cancer cell metabolism to metastasis, Dis. Model Mech. 11 (2018) dmm032920, , https://doi.org/10.1242/dmm.032920.

[11] C. Vernieri, S. Casola, M. Foiani, F. Pietrantonio, F. de Braud, V. Longo, Targeting cancer metabolism: dietary and pharmacologic interventions, Cancer Discov. 6 (2016) 1315–1333, https://doi.org/10.1158/2159-8290.CD-16-0615.

[12] J.L. Kovar, W. Volcheck, E. Sevick-Muraca, M.A. Simpson, D.M. Olive, Characterization and performance of a near-infrared 2-deoxyglucose optical imaging agent for mouse cancer models, Anal. Biochem. 384 (2009) 254–262, https://doi.org/10.1016/j.ab.2008.09.050.

[13] K.E. Adams, S. Ke, S. Kwon, F. Liang, Z. Fan, Y. Lu, K. Hirschi, M.E. Mawad, M.A. Barry, E.M. Sevick-Muraca, Comparison of visible and near-infrared wavelength-excitable fluorescent dyes for molecular imaging of cancer, J. Biomed. Opt. 12 (2007) 024017, , https://doi.org/10.1117/1.2717137.

[14] H. Zhou, K. Luby-Phelps, B.E. Mickey, A.A. Habib, R.P. Mason, D. Zhao, Dynamic near-infrared optical imaging of 2-deoxyglucose uptake by intracranial glioma of athymic mice, PLoS One 4 (2009) e8051, https://doi.org/10.1371/journal.pone.0008051.

[15] I.M. Mol, B.-W. Xie, E.R. van Beek, T.J.A. Snoeks, A. Chan, C.W.G.M. Löwik, S. Keereweer, I. Que, E.L. Kaijzel, Dual-wavelength imaging of tumor progression by activatable and targeting near-infrared fluorescent probes in a bioluminescent breast cancer model, PLoS One 7 (2012) e31875, https://doi.org/10.1371/journal.pone.0031875.

[16] E.C. Nakajima, C. Laymon, M. Oborski, W. Hou, L. Wang, J.R. Grandis, R.L. Ferris, J.M. Mountz, B. Van Houten, Quantifying metabolic heterogeneity in head and neck tumors in real time: 2-DG uptake is highest in hypoxic tumor regions, PLoS One 9 (2014) e102452, , https://doi.org/10.1371/journal.pone.0102452.

[17] J.S. Desgrosellier, D.A. Cheresh, Integrins in cancer: biological implications and therapeutic opportunities, Nat. Rev. Cancer. 10 (2010) 9–22, https://doi.org/10.1038/nrc2748.

[18] S. Shishido, H. Bonig, Y.-M. Kim, Role of integrin Alpha4 in drug resistance of leukemia, Front. Oncol. 4 (2014) 99, https://doi.org/10.3389/fonc.2014.00099.

[19] N. Matsuura, W. Puzon-McLaughlin, A. Irie, Y. Morikawa, K. Kakudo, Y. Takada, Induction of experimental bone metastasis in mice by transfection of integrin alpha 4 beta 1 into tumor cells, Am. J. Pathol. 148 (1996) 55–61 http://www.ncbi.nlm.nih.gov/pubmed/8546226.

[20] W.J. Akers, D. Soodgupta, W. Beaino, L. Lu, R. Laforest, M. Shokeen, J. Skeath, C.J. Anderson, M. Rettig, M. Snee, H. Zhou, M.H. Tomasson, J.F. DiPersio, Ex vivo and in vivo evaluation of overexpressed VLA-4 in multiple myeloma using LLP2A imaging agents, J. Nucl. Med. 57 (2016) 640–645, https://doi.org/10.2967/jnumed.115.164624.

[21] L. Peng, R. Liu, J. Marik, X. Wang, Y. Takada, K.S. Lam, Combinatorial chemistry identifies high-affinity peptidomimetics against α4β1 integrin for *in vivo* tumor imaging, Nat. Chem. Biol. 2 (2006) 381–389, https://doi.org/10.1038/nchembio798.

[22] K.S. Lam, R. Liu, W. Xiao, M. Andrei, L. Peng, *In vivo* optical imaging of human lymphoma xenograft using a library-derived peptidomimetic against α4β1 integrin, Mol. Cancer Ther. 7 (2008) 432–437, https://doi.org/10.1158/1535-7163.mct-07-0575.

[23] G. Pagnucco, G. Cardinale, F. Gervasi, Targeting multiple myeloma cells and their bone marrow microenvironment, Ann. N. Y. Acad. Sci. 1028 (2004) 390–399, https://doi.org/10.1196/annals.1322.047.

[24] L. Seguin, J.S. Desgrosellier, S.M. Weis, D.A. Cheresh, Integrins and cancer: regulators of cancer stemness, metastasis, and drug resistance, Trends Cell Biol. 25 (2015) 234–240, https://doi.org/10.1016/j.tcb.2014.12.006.

[25] J.S. Damiano, A.E. Cress, L.A. Hazlehurst, A.A. Shtil, W.S. Dalton, Cell adhesion mediated drug resistance (CAM-DR): role of integrins and resistance to apoptosis in human myeloma cell lines, Blood 93 (1999) 1658–1667.

[26] T. Lapidot, How do stem cells find their way home? Blood 106 (2005) 1901–1910, https://doi.org/10.1182/blood-2005-04-1417.

[27] P. De La Puente, B. Muz, F. Azab, A.K. Azab, Cell trafficking of endothelial progenitor cells in tumor progression, Clin. Cancer Res. 19 (2013) 3360–3368, https://doi.org/10.1158/1078-0432.CCR-13-0462.

[28] K. Raymaekers, S. Stegen, N. van Gastel, G. Carmeliet, The vasculature: a vessel for bone metastasis, Bonekey Rep. 742 (2015) 1–7, https://doi.org/10.1038/bonekey.2015.111.

[29] K. Vandoorne, D. Rohde, H.Y. Kim, G. Courties, G. Wojtkiewicz, L. Honold, F.F. Hoyer, V. Frodermann, R. Nayar, F. Herisson, Y. Jung, P.A. Désogère, C. Vinegoni, P. Caravan, R. Weissleder, D.E. Sosnovik, C.P. Lin, F.K. Swirski, M. Nahrendorf, Imaging the vascular bone marrow niche during inflammatory stress, Circ. Res. 123 (2018) 415–427, https://doi.org/10.1161/CIRCRESAHA.118.313302.

[30] J.M. Runnels, A.L. Carlson, C. Pitsillides, B. Thompson, J. Wu, J.A. Spencer, J.M.J. Kohler, A. Azab, A.-S. Moreau, S.J. Rodig, A.L. Kung, K.C. Anderson, I.M. Ghobrial, C.P. Lin, Optical techniques for tracking multiple myeloma engraftment, growth, and response to therapy, J. Biomed. Opt. 16 (2011) 011006, , https://doi.org/10.1117/1.3520571.

[31] X. Jia, A.M. Roccaro, A.K. Azab, M.R. Melhem, C. Pitsillides, A.-S. Moreau, M. Farag, R. Wright, X. Leleu, C.P. Lin, A.L. Carlson, K.C. Anderson, A. Sacco, B.J. Rollins, J.M. Runnels, T. Hideshima, N.C. Munshi, F. Azab, B. Ospina, A.L. Kung, H.T. Ngo, I.M. Ghobrial, C. Alt, N. Burwick, CXCR4 inhibitor AMD3100 disrupts the interaction of multiple myeloma cells with the bone marrow microenvironment and enhances their sensitivity to therapy, Blood 113 (2009) 4341–4351, https://doi.org/10.1182/blood-2008-10-186668.

[32] F.M. Lambers, G. Kuhn, R. Müller, Advances in multimodality molecular imaging of bone structure and function, Bonekey Rep. 1 (2012) 1–8, https://doi.org/10.1038/bonekey.2012.28.

[33] K.M. Kozloff, R. Weissleder, U. Mahmood, Noninvasive optical detection of bone mineral, J. Bone Miner. Res. 22 (2007) 1208–1216, https://doi.org/10.1359/jbmr.070504.

[34] K.M. Kozloff, L.I. Volakis, J.C. Marini, M.S. Caird, Near-infrared fluorescent probe traces bisphosphonate delivery and retention *in vivo*, J. Bone Miner. Res. 25 (2010) 1748–1758, https://doi.org/10.1002/jbmr.66.

[35] E. Golub, L. Qing, D. Wen, S. Akintoye, G. Harrison, Anatomic site variability in rat skeletal uptake and desorption of fluorescently labeled bisphosphonate, Oral Dis 17 (2010) 427–432, https://doi.org/10.1111/j.1601-0825.2010.01772.x.

[36] C.J. Galbán, B.A. Hoff, K. Chughtai, B.D. Ross, Y.H. Jeon, A. Rehemtulla, K. Kozloff, S. Galbán, Multimodality imaging of tumor and bone response in a mouse model of bony metastasis, Transl. Oncol. 5 (2014) 415–421, https://doi.org/10.1593/tlo.12298.

[37] S. Junankar, G. Shay, J. Jurczyluk, N. Ali, J. Down, N. Pocock, A. Parker, A. Nguyen, S. Sun, B. Kashemirov, C.E. McKenna, P.I. Croucher, A. Swarbrick, K. Weilbaecher, T.G. Phan, M.J. Rogers, Real-time intravital imaging establishes tumor-associated macrophages as the extraskeletal target of bisphosphonate action in cancer, Cancer Discov. 5 (2015) 35–42, https://doi.org/10.1158/2159-8290.CD-14-0621.

[38] T. Imamura, T. Saitou, R. Kawakami, *In vivo* optical imaging of cancer cell function and tumor microenvironment, Cancer Sci. 109 (2018) 912–918, https://doi.org/10.1111/cas.13544.

[39] S. Filippini, M.W. Starbuck, D.W. Hutmacher, S. Alexander, P. Friedl, E.M. De-Juan-

Pardo, C.J. Logothetis, E. Dondossola, R.M. Hoffman, B.M. Holzapfel, N. Navone, Intravital microscopy of osteolytic progression and therapy response of cancer lesions in the bone, Sci. Transl. Med. 10 (2018) eaao5726, https://doi.org/10.1126/scitranslmed.aao5726.

[40] N.P. Withana, G. Blum, M. Sameni, C. Slaney, A. Anbalagan, M.B. Olive, B.N. Bidwell, L. Edgington, L. Wang, K. Moin, B.F. Sloane, R.L. Anderson, M.S. Bogyo, B.S. Parker, Cathepsin b inhibition limits bone metastasis in breast cancer, Cancer Res. 72 (2012) 1199–1209, https://doi.org/10.1158/0008-5472.CAN-11-2759.

[41] R. Baron, S. Ferrari, R.G.G. Russell, Denosumab and bisphosphonates: different mechanisms of action and effects, Bone 48 (2011) 677–692, https://doi.org/10.1016/j.bone.2010.11.020.

[42] P.H. Stern, Antiresorptive agents and osteoclast apoptosis, J. Cell. Biochem. 101 (2007) 1087–1096, https://doi.org/10.1002/jcb.21311.

[43] S. Khosla, D. Burr, J. Cauley, D.W. Dempster, P.R. Ebeling, D. Felsenberg, R.F. Gagel, V. Gilsanz, T. Guise, S. Koka, L.K. McCauley, J. McGowan, M.D. McKee, S. Mohla, D.G. Pendrys, L.G. Raisz, S.L. Ruggiero, D.M. Shafer, L. Shum, S.L. Silverman, C.H. Van Poznak, N. Watts, S. Bin Woo, E. Shane, Bisphosphonate-associated osteonecrosis of the jaw: report of a task force of the american society for bone and mineral research, J. Bone Miner. Res. 22 (2007) 1479–1491, https://doi.org/10.1359/jbmr.0707onj.

[44] J.L. Kovar, X. Xu, D. Draney, A. Cupp, M.A. Simpson, D. Michael Olive, Near-infrared-labeled tetracycline derivative is an effective marker of bone deposition in mice, Anal. Biochem. 416 (2011) 167–173, https://doi.org/10.1016/j.ab.2011.05.011.

[45] F.S. Ward, M.S. Caird, B. Meyer, K. Cortright, T.N. Jenks, B.P. Sinder, D.K. Barton, B.M. Khoury, K.M. Kozloff, J.C. Marini, J.E. Perosky, Single dose of bisphosphonate preserves gains in bone mass following cessation of sclerostin antibody in Brtl/+ osteogenesis imperfecta model, Bone 93 (2016) 79–85, https://doi.org/10.1016/j.bone.2016.09.013.

[46] C.A. Foss, D. Bedja, R.C. Mease, H. Wang, D.A. Kass, S. Chatterjee, M.G. Pomper, Molecular imaging of inflammation in the ApoE -/- mouse model of atherosclerosis with IodoDPA, Biochem. Biophys. Res. Commun. 461 (2015) 70–75, https://doi.org/10.1016/j.bbrc.2015.03.171.

[47] M.J.C. Moester, M.A.E. Schoeman, I.B. Oudshoorn, M.M. van Beusekom, I.M. Mol, E.L. Kaijzel, C.W.G.M. Löwik, K.E. De Rooij, Validation of a simple and fast method to quantify in vitro mineralization with fluorescent probes used in molecular imaging of bone, Biochem. Biophys. Res. Commun. 443 (2014) 80–85, https://doi.org/10.1016/j.bbrc.2013.11.055.

[48] K.M. Harmatys, E.L. Cole, B.D. Smith, In vivo imaging of bone using a deep-red fluorescent molecular probe bearing multiple iminodiacetate groups, Mol. Pharm. 10 (2013) 4263–4271, https://doi.org/10.1021/mp400357v.

[49] L. Pes, Y. Kim, C.H. Tung, Bidentate iminodiacetate modified dendrimer for bone imaging, Bioorganic Med. Chem. Lett. 27 (2017) 1252–1255, https://doi.org/10.1016/j.bmcl.2017.01.059.

[50] J.O. Deguchi, M. Aikawa, C.H. Tung, E. Aikawa, D.E. Kim, V. Ntziachristos, R. Weissleder, P. Libby, Inflammation in atherosclerosis: visualizing matrix metalloproteinase action in macrophages in vivo, Circulation 114 (2006) 55–62, https://doi.org/10.1161/CIRCULATIONAHA.106.619056.

[51] E. Gounaris, C.H. Tung, C. Restaino, R. Maehr, R. Kohler, J.A. Joyce, H.L. Plough, T.A. Barrett, R. Weissleder, K. Khazaie, Live imaging of cysteine-cathepsin activity reveals dynamics of focal inflammation, angiogenesis, and polyp growth, PLoS One 3 (2008), https://doi.org/10.1371/journal.pone.0002916.

[52] M. Shibutani, S. Kemmochi, Y. Ishihara, N. Onda, R. Morita, In vivo imaging of tissue-remodeling activity involving infiltration of macrophages by a systemically administered protease-activatable probe in colon cancer tissues, Transl. Oncol. 6 (2014), https://doi.org/10.1593/tlo.13430 628-IN4.

[53] K.M. Kozloff, L. Quinti, S. Patntirapong, P.V. Hauschka, C.H. Tung, R. Weissleder, U. Mahmood, Non-invasive optical detection of cathepsin K-mediated fluorescence reveals osteoclast activity in vitro and in vivo, Bone 44 (2009) 190–198, https://doi.org/10.1016/j.bone.2008.10.036.

[54] P.B. Satkunananthan, M.J. Anderson, N.M. De Jesus, D.R. Haudenschild, C.M. Ripplinger, B.A. Christiansen, Invivo fluorescence reflectance imaging of protease activity in a mouse model of post-traumatic osteoarthritis, Osteoarthr. Cartil. 22 (2014) 1461–1469, https://doi.org/10.1016/j.joca.2014.07.011.

[55] B. Fingleton, M. Futakuchi, A. Hikosaka, T.C. Vargo-Gogola, L.M. Matrisian, T. Shirai, N. Kawai, J.L. Begtrup, M.D. Martin, R.K. Singh, H.B. Acuff, T.E. Peterson, C.C. Lynch, MMP-7 promotes prostate cancer-induced osteolysis via the solubilization of RANKL, Cancer Cell 7 (2005) 485–496, https://doi.org/10.1016/j.ccr.2005.04.013.

[56] K. Kessenbrock, V. Plaks, Z. Werb, Matrix Metalloproteinases, Regulators of the tumor microenvironment, Cell 141 (2010) 52–67, https://doi.org/10.1016/j.cell.2010.03.015.

[57] V. Ntziachristos, C.H. Tung, C. Bremer, R. Weissleder, Fluorescence molecular tomography resolves protease activity in vivo, Nat. Med. 8 (2002) 757–760, https://doi.org/10.1038/nm729.

[58] T. Fukui, E. Tenborg, J.H.N. Yik, D.R. Haudenschild, In-vitro and in-vivo imaging of MMP activity in cartilage and joint injury, Biochem. Biophys. Res. Commun. 460 (2015) 741–746, https://doi.org/10.1016/j.bbrc.2015.03.100.

[59] M.D. Morris, G.S. Mandair, Raman assessment of bone quality, Clin. Orthop. Relat. Res. 469 (2011) 2160–2169, https://doi.org/10.1007/s11999-010-1692-y.

[60] M. Khalid, T. Bora, A. Al Ghaithi, S. Thukral, J. Dutta, Raman spectroscopy detects changes in bone mineral quality and collagen cross-linkage in staphylococcus infected human bone, Sci. Rep. 8 (2018) 1–9, https://doi.org/10.1038/s41598-018-27752-z.

[61] W.F. Finney, D. Sudhaker Rao, E. Widjaja, S.A. Goldstein, B.R. McCreadie, T. Chen,

[62] C. Zhang, P.T. Winnard, S. Dasari, S.L. Kominsky, M. Doucet, S. Jayaraman, V. Raman, I. Barman, Label-free Raman spectroscopy provides early determination and precise localization of breast cancer-colonized bone alterations, Chem. Sci. 9 (2018) 743–753, https://doi.org/10.1039/c7sc02905e.

[63] M.V. Burke, A. Atkins, M. Akens, T.L. Willett, C.M. Whyne, Osteolytic and mixed cancer metastasis modulates collagen and mineral parameters within rat vertebral bone matrix, J. Orthop. Res. 34 (2016) 2126–2136, https://doi.org/10.1002/jor.23248.

[64] X. Bi, J.A. Sterling, A.R. Merkel, D.S. Perrien, J.S. Nyman, A. Mahadevan-Jansen, Prostate cancer metastases alter bone mineral and matrix composition independent of effects on bone architecture in mice - A quantitative study using microCT and raman spectroscopy, Bone 56 (2013) 454–460, https://doi.org/10.1016/j.bone.2013.07.006.

[65] J. Kolmas, D. Marek, W. Kolodziejski, Near-infrared (NIR) spectroscopy of synthetic hydroxyapatites and human dental tissues, Appl. Spectrosc. 69 (2015) 902–912, https://doi.org/10.1366/14-07720.

[66] C.S. Rajapakse, M.V. Padalkar, H.J. Yang, M. Ispiryan, N. Pleshko, Non-destructive NIR spectral imaging assessment of bone water: comparison to MRI measurements, Bone 103 (2017) 116–124, https://doi.org/10.1016/j.bone.2017.06.015.

[67] W.D. Strain, R. Meertens, C. Thorn, K.M. Knapp, F. Casanova, Use of near-infrared systems for investigations of hemodynamics in human in vivo bone tissue: a systematic review, J. Orthop. Res. 36 (2018) 2595–2603, https://doi.org/10.1002/jor.24035.

[68] V.R. Kondepati, H.M. Heise, J. Backhaus, Recent applications of near-infrared spectroscopy in cancer diagnosis and therapy, Anal. Bioanal. Chem. 390 (2008) 125–139, https://doi.org/10.1007/s00216-007-1651-y.

[69] J. Xia, J. Yao, L.V. Wang, PhotoAcoustic tomography: principles and advances, Electromagn. Waves 147 (2014) 1–22, https://doi.org/10.2528/PIER14032303.

[70] K.S. Valluru, K.E. Wilson, J.K. Willmann, PhotoAcoustic imaging in oncology: translational preclinical and early clinical experience, Radiology 280 (2016) 332–349, https://doi.org/10.1148/radiol.16151414.

[71] T. Imai, B. Muz, C.H. Yeh, J. Yao, R. Zhang, A.K. Azab, L. Wang, Direct measurement of hypoxia in a xenograft multiple myeloma model by optical-resolution photoacoustic microscopy, Cancer Biol. Ther. 18 (2017) 101–105, https://doi.org/10.1080/15384047.2016.1276137.

[72] J.A. Viator, C.W. Caldwell, P.S. Dale, R.M. Weight, A.E. Lisle, PhotoAcoustic detection of metastatic melanoma cells in the human circulatory system, Opt. Lett. 31 (2006) 2998, https://doi.org/10.1364/ol.31.002998.

[73] E.I. Galanzha, E.V. Shashkov, P.M. Spring, J.Y. Suen, V.P. Zharov, In vivo, non-invasive, label-free detection and eradication of circulating metastatic melanoma cells using two-color photoacoustic flow cytometry with a diode laser, Cancer Res. 69 (2009) 7926–7934, https://doi.org/10.1158/0008-5472.CAN-08-4900.

[74] M.A. Juratli, M. Sarimollaoglu, E.R. Siegel, D.A. Nedosekin, E.I. Galanzha, J.Y. Suen, V.P. Zharov, Real-time monitoring of circulating tumor cell release during tumor manipulation using in vivo photoacoustic and fluorescent flow cytometry, Head Neck 36 (2014) 1207–1215, https://doi.org/10.1002/hed.23439.

[75] M.L. Li, J.T. Oh, X. Xie, G. Ku, W. Wang, C. Li, G. Lungu, G. Stoica, L.V. Wang, Simultaneous molecular and hypoxia imaging of brain tumors in vivo using spectroscopic photoacoustic tomography, Proc. IEEE 96 (2008) 481–489, https://doi.org/10.1109/JPROC.2007.913515.

[76] J. Levi, A. Sathirachinda, S.S. Gambhir, A high-affinity, high-stability photoacoustic agent for imaging gastrin-releasing peptide receptor in prostate cancer, Clin. Cancer Res. 20 (2014) 3721–3729, https://doi.org/10.1158/1078-0432.CCR-13-3405.

[77] G. Ku, L.V. Wang, Deeply penetrating photoacoustic tomography in biological tissues enhanced with an optical contrast agent, Opt. Lett. 30 (2005) 507, https://doi.org/10.1364/ol.30.000507.

[78] G. Stoica, X. Wang, G. Ku, M.A. Wegiel, L.V. Wang, D.J. Bornhop, Noninvasive photoacoustic angiography of animal brains in vivo with near-infrared light and an optical contrast agent, Opt. Lett. 29 (2004) 730, https://doi.org/10.1364/ol.29.000730.

[79] W Li., X. Chen, Gold nanoparticles for photoacoustic imaging, Nanomedicine 10 (2015) 299–320, https://doi.org/10.2217/nnm.14.169.

[80] D.L. Chamberland, A. Agarwal, N. Kotov, J. Brian Fowlkes, P.L. Carson, X. Wang, PhotoAcoustic tomography of joints aided by an etanercept-conjugated gold nanoparticle contrast agent - An ex vivo preliminary rat study, Nanotechnology (2008) 19, https://doi.org/10.1088/0957-4484/19/9/095101.

[81] J. Hu, M. Yu, F. Ye, D. Xing, In vivo photoacoustic imaging of osteosarcoma in a rat model, J. Biomed. Opt. 16 (2011) 020503, , https://doi.org/10.1117/1.3544502.

[82] Z. Ma, H. Qin, H. Chen, H. Yang, J. Xu, S. Yang, J. Hu, D. Xing, Phage display-derived oligopeptide-functionalized probes for in vivo specific photoacoustic imaging of osteosarcoma, Nanomed. Nanotechnol., Biol. Med. 13 (2017) 111–121, https://doi.org/10.1016/j.nano.2016.09.002.

[83] D.L. Chamberland, X. Wang, B.J. Roessler, PhotoAcoustic tomography of carrageenan-induced arthritis in a rat model, J. Biomed. Opt. 13 (2008) 011005, , https://doi.org/10.1117/1.2841028.

[84] J. Shubert, M.A. Lediju Bell, PhotoAcoustic imaging of a human vertebra: implications for guiding spinal fusion surgeries, Phys. Med. Biol 63 (2018) 0–13, https://doi.org/10.1088/1361-6560/aacdd3.

[85] T. Feng, X. Wang, C. Tian, J. Yuan, Y.-S. Hsiao, C.X. Deng, S. Du, K.M. Kozloff, J.E. Perosky, Bone assessment via thermal photo-acoustic measurements, Opt. Lett. 40 (2015) 1721, https://doi.org/10.1364/ol.40.001721.

[86] S.M. Devine, N. Flomenberg, D.H. Vesole, J. Liesveld, D. Weisdorf, K. Badel, G. Calandra, J.F. DiPersio, Rapid mobilization of CD34 + cells following

administration of the CXCR4 antagonist AMD3100 to patients with multiple myeloma and non-Hodgkin's lymphoma, J. Clin. Oncol. 22 (2004) 1095–1102, https://doi.org/10.1200/JCO.2004.07.131.

[87] D. Santini, S. Galluzzo, A. Zoccoli, F. Pantano, M.E. Fratto, B. Vincenzi, L. Lombardi, C. Gucciardino, N. Silvestris, E. Riva, S. Rizzo, A. Russo, E. Maiello, G. Colucci, G. Tonini, New molecular targets in bone metastases, Cancer Treat. Rev. 36 (2010) S6–S10, https://doi.org/10.1016/S0305-7372(10)70013-X.

[88] F. Leblond, M.-C. Guiot, M. Jermyn, K. Mok, J. Desroches, J. Mercier, L. Bernstein, K. Saint-Arnaud, J. Pichette, K. Petrecca, Intraoperative brain cancer detection with raman spectroscopy in humans, Sci. Transl. Med. 7 (2015), https://doi.org/10.1126/scitranslmed.aaa2384 274ra19-274ra19.

[89] L. Lin, P. Hu, J. Shi, C.M. Appleton, K. Maslov, L. Li, R. Zhang, L.V. Wang, Single-breath-hold photoacoustic computed tomography of the breast, Nat. Commun. 9 (2018), https://doi.org/10.1038/s41467-018-04576-z.